2024 10th IEEE RAS/EMBS International Conference for
Biomedical Robotics and Biomechatronics (BioRob)
1-4 September 2024. Heidelberg, Germany

Computational Design Optimization of Concentric Tube Robots for Patient-Specific Volumes and End Effector Tasks

A.G. de Groot[1], M.K. Welleweerd[1], E.B. Cornel[2], V. Groenhuis[1], S. Stramigioli[1], F.J. Siepel[1]

***Abstract*— Concentric Tube Robots (CTRs) show high potential as patient- and task-specific minimally invasive robots, as their workspace can be optimized for task completion in confined workspaces such as the human bladder. Ensuring high-quality task completion at regions of interest on the bladder wall, however, requires precise positioning and orienting of imaging devices or tooling relative to the bladder wall.**

To this end, we present an optimization framework for the design parameters of the CTR which not only considers position, but also orientation of the CTR End-Effector (EE) with respect to the task surface. This ensures that the EE-task can be performed under the set constraints at the desired task surface within a given workspace.

Our results show the coverage of five EE-tasks over two task surfaces; a simplified model of the lower urinary tract (urethra and bladder) and an anatomically correct model based on MR-image segmentation. Optimization focused solely on positioning yields a notable 94.2% reduction in task surface coverage when orientational considerations are incorporated into the EE-task. Moreover, the introduction of an alternative orientation for the EE-task results in an 18% decrease in coverage. Therefore, we conclude that task optimization should be performed based on both the position and orientation of the EE with respect to the task surface.

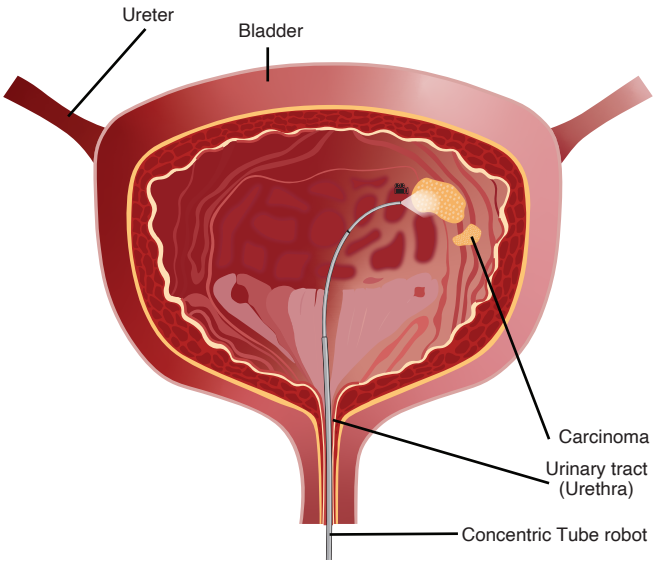

Fig. 1: Schematic overview of the bladder, urethra and the CTR performing a visualization of the bladder wall.

I. Introduction

The human body contains multiple hollow structures, such as the lower urinary tract, colon, and trachea, through which visualization or surgical tools are guided. During laparoscopic procedures, a hollow space is created in the body to improve maneuverability of the laparoscopic tools. These volumes can be exploited during robotic-guided minimally invasive surgery as they create a patient-specific workspace in which to perform a task, such as visualization of organs or tumors.

We investigate robotic-assisted surgery in bladder cancer and therefore, we select the bladder as hollow structure. However, this approach can be extrapolated to other patient-specific volumes or diseases. Bladder cancer is one of the ten most common cancer types worldwide with a lifetime risk of 1.1% for men and 0.27% for women [1]. Diagnosis of bladder cancer starts with a cystoscopy to visually inspect the urethra and bladder wall. This inspection is performed using a rigid or flexible endoscope and is important not only for the diagnosis but also for the treatment and monitoring of bladder cancer later on. However, regions of interest are documented in written form during visualization of the bladder wall, which can lead to miscommunication between clinicians during follow-up procedures [2].

Digital mapping of the bladder can reduce follow-up communication errors about locations of regions of interests between clinicians [2], [3]. As clinicians can review previous digital maps to approximate their current location in respect to the location of region of interest of previous digital maps. These digital maps can also be improved with advanced imaging techniques such as optical coherence tomography (OCT). OCT provides a 4 µm lateral, a 3 µm axial resolution, and a depth penetration of up to 5 mm [4]. With a bladder wall thickness of 3 mm for bladder volumes comparable to cystoscopy bladder fillings [5], these high-resolution OCT images have the potential to eliminate the need for a physical biopsy. As OCT images provide instant discriminate between healthy tissue and non-muscular and muscular invasive tumors, which helps determine the appropriate treatment trajectory.

During a cystoscopy a rigid or flexible endoscope, which is a single-stage handheld tendon driven manipulator, is used to visually inspect the bladder wall. However, these handheld endoscopes have limited capabilities to position the OCT system at the optimal point relative to the bladder wall. Correct positioning of the OCT system is essential; non-orthogonality and deviations from the optimal distance to the tissue reduce the penetration depth. This reduces

This project has received funding from OPoost an European fund for regional development under the name Next gen in-vivo cancer diagnostics.

[1] is affiliated with the Robotics and Mechatronics group, University of Twente, The Netherlands. a.g.degroot@utwente.nl

[2] is affiliated with Andros Clinics, Arnhem, The Netherlands.

the effectiveness of the OCT images by impairing the discrimination between non-muscular and muscular tumors, which is vital for determining the optimal follow-up treatment.

Concentric tube robots (CTRs) consist of two or more pre-curved superelastic tubes nested in each other and are actuated by axial rotation and translation of the individual tubes. CTRs are well suited to navigating confined spaces such as a body cavity because of their slender, needle-like shape and compliant body. Additionally, the hollow inner structure of CTRs provides a work channel from the proximal to the distal end, or end effector (EE), of the CTR. This work channel can be exploited to bring tooling such as imaging devices or grippers to the surgical site making CTRs inherently suited for robotic-assisted minimally invasive surgery.

The workspace of a CTR, defined as all reachable EE poses, is a product of the elastic interaction between the three design parameters of each individual tube and the set of all actuations defined as the configuration space. The length of the straight and curved section, and the radius of the curved section create a highly configurable and more elaborate workspace than tendon driven flexible endoscopes have [6]. However, the mapping between the configuration space and the workspace is complex because of the elastic interaction between the pre-curved tubes [7], [8]. Therefore, it is challenging to find the design parameters that allow the robot to navigate confined workspaces and perform a task within this given workspace.

Several computational frameworks either optimize the design parameters to reach a given point in space or shape the CTR workspace to match the desired workspace while avoiding tissue interaction. Bergeles et al. [9] presented a point-to-point methodology with a set of design parameters and configuration sets. The curve of the individual tubes can be fixed or variable. Lin et al. [10] extends the point-to-point methodology by adding a motion planner to enable safe navigation towards the target point. In another approach, Burgner et al. [11] presented a volume-based method that maximizes the overlap between the actual and the desired workspace by a grid search through the configuration space to calculate the overlap and a Nelder-Mead simplex algorithm to optimize the design parameters. Baykal et al. [12] reduced the computation time from days to hours by calculating the overlap with a rapidly-exploring random tree (RRT) [13] in the configuration space and optimizing the design parameters with an Adaptive Simulated Annealing (ASA) algorithm [14]. They also allowed for interchangeable tube set configurations to ensure near-perfect overlap of the desired workspace.

These existing approaches optimize the design parameters to ensure proper matching of the EE position but do not consider the orientation. However, the tool's orientation is equally important, so reaching a position does not guarantee effective use of the EE. An example is the visualization of the bladder wall; not only should the EE be in a particular position but also the camera should be orientated towards the bladder wall. In summary, an EE task is defined not only by position but also by orientation. Additionally, this also means that the EE task needs to be performed in respect to a surface area rather than ad a single point within the workspace.

To address this problem, we present an optimization framework that considers both the EE's position and orientation with respect to the tissue surface at which the EE task has to be performed during computational design.

II. Methods

Considering our case study; the visual inspection of the bladder wall for possible tumors (see Fig. 1). The CTR should first navigate through the urethra to the bladder and then start the visual inspection of the bladder wall. Then, while operating within the bladder, the EE pose of the CTR should be within the set task constraints in respect to the bladder wall e.g., within the focal distance of the camera to ensure high-quality image acquisition. Furthermore, the complete bladder wall should be imaged to ensure a high-quality inspection. Therefore, the design parameters of the individual CTR tubes should be optimized to maximize the task coverage over the set task surface under the EE task constraints.

The method section describes: first, the body cavity is described in which the CTR operates and navigates. Second, the design parameters which are optimized, and the structural parameters of the tubes are described. Third, the EE parameters are described which form the task constraints for the given task the CTR should perform and finally the optimization framework is described which uses these parameter sets to optimize the CTR design parameters for a given task within a body cavity.

A. Body cavity

The body cavity in which the CTR operates is a volume enclosed by tissue surfaces and consists of two parts: the path towards the body cavity and the body cavity itself. The path can start from either a natural or surgical body orifice. The task surface at which the EE task is performed is defined as the tissue which encloses the body cavity. The overall shape of the path and body cavity could be based on medical images or a simplified representation of existing body cavities.

Computationally the body cavity is described by triangulating the path and task surface in three edge faces. Therefore, each face and its normal vector represent a given tissue area and the normal vector of the represented tissue area. The accuracy of the framework increases as the face area decreases, but the computation time will also increase.

The two presented body cavities are of the urethra and bladder: body cavity A (Fig. 2a) is a simplified model and body cavity B (Fig. 2b) is a model based on MRI segmentation. The urethra forms the path leading to the bladder, and the bladder wall is the task surface at which the EE task is performed. For body cavity A, the urethra is simplified to a cylinder with a diameter of 15 mm and a length of 30 mm and the bladder to a sphere with a diameter of 100 mm. Body cavity B is based on MRI segmentation of 128 T2-weighted MR-slices with a voxel dimension of $0.88 \times 0.88 \times 1.0$ mm. The contours of the inner bladder wall are segmented manual in MevisLab (Mevis Medical

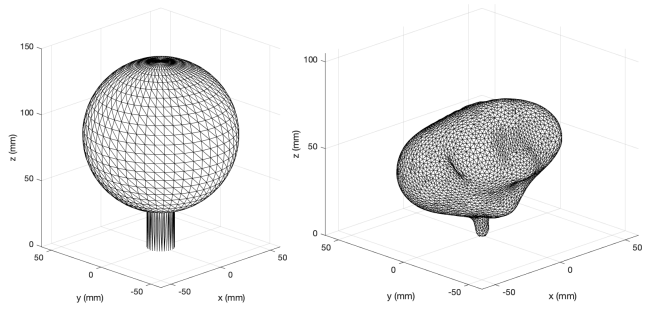

Fig. 2: Triangulated representation of the urethra and bladder models in which the CTR operates with a) the simplified model and b) the MRI segmented model.

Solutions, Bremen, Germany) based on the high gradient difference between the water contained in the bladder and the inner bladder wall. MevisLab then creates a mesh based on the segmented contours of the individual MR-slices [15]. The resulting dimensions of the MRI segmented model are 120×110×85 mm (l×w×h), resulting in 500 mL bladder volume which is similar as the bladder volume of the simplified model. Both models are built up out of three edge faces and have a maximum face area of 10.2 mm^2.

B. Design parameters

Each CTR tube has two configurable design parameters and four fixed parameters. The two configurable design parameters are the length of the curved section (L_c) and the radius of the curvature (κ). However, the radius of the curvature has a lower bound to ensure that the tube does not deform or buckle during actuation. The minimum radius is bounded by the outer tube diameter (OD) and the material strain (ε), this results in the following lower bound equation [16]:

$$\kappa_l = \frac{2\varepsilon}{OD(1+\varepsilon)} \tag{1}$$

with κ_l the lower bound of the radius of curvature for a given outer tube diameter. Note that smaller tube diameters can sustain a smaller radius, but larger tube radii reduce bi-fracture effects [16].

The four fixed parameters are the maximum material strain of the tube, the inner and outer tube diameter, and the overall length of the tube. Previous studies mainly presented CTR tubes fabricated from Nitinol, a superelastic material with a recoverable strain of $8-10\%$, Young's modulus of 50 GPa and a Poisson's ratio of 0.3 [17]. Therefore, the simulated CTR tubes will be using Nitinol's characteristics. The individual tube dimensions (inner and outer diameter) mainly depend on the EE task, as tooling should pass through the work channel set by the inner diameter of the most inner tube. Consequently by setting the diameter of most inner tube based on the EE task requirements the other tube diameters are also roughly set. Therefore, this study pre-selects the tube dimensions while Lin et al. [10], optimizes these tube dimensions. This study presents a visualization task and therefore the most inner tubes must house a camera system with a diameter of 1.6 mm, resulting in the following tube parameters during simulation: Table I. The total tube length is the length of the curved section plus the length of the straight section and is chosen such that the robot can reach all positions in the body cavity.

TABLE I: The inner and outer diameter of the simulated tubes, with tube 1 the most inner tube.

Tube	Inner diameter (mm)	Outer diameter (mm)
1	1.72	2.32
2	2.68	3.28
3	3.72	5.72

C. End effector parameters

The simulated EE task is the visualization of the bladder wall, this task is performed with four different EE configurations ($EE_{ci}, i = 1,2,...,n$). Each EE configuration is described by five constraints and three structural parameters which allow for a general task description making the framework applicable for a large range of EE tasks.

The five EE constraints are: minimum (r_{min}) and maximum (r_{max}) distance between the task surface and EE measured along the task orientation vector (red arrow; Fig. 3), the angle between the task surface normal vector and the task orientation vector in both the x- (α_x) and y-plane (α_y) of the task surface frame and the angle of the field of operation (β) of the EE task. In addition, three structural EE parameters are defined: the operating angle (γ), which is defined as the offset between the axial axis of the most inner tube and the axis of the task orientation vector. Second, the ability of the EE to rotate within the most inner tube as this results in a larger effective workspace for EE-tasks with an operating offset. Finally, the length of the EE (EE_l) measured along the axial axis of the CTR body. The relation between these constraints and the task surface is shown in Fig. 3.

Rigid and flexible endoscopes used during cystoscopy mainly use forward facing cameras ($\gamma = 0°$), but other operating angles (γ) are available. Therefore, we present a EE task which should visualize the bladder wall with a single camera system, but each EE configuration (EE_{ci}) has a different operating angle (γ). The four operating angles are for EE_{c1}; 0° (forward facing camera), EE_{c2}; 15°, EE_{c3}; 45° and EE_{c4}; 90° (sideways facing camera). The remaining parameters of the camera system are: r_{min} is 9 mm, r_{max} is 11 mm (focus distance camera), $\alpha_x = \alpha_y$ is 5° and β is 90°. The camera system protrudes 10 mm (EE_l) out of the CTR body and has the ability to rotate within the hollow CTR structure.

Additionally, a second EE task and thereby a fifth EE configuration (EE_{c5}) is presented. The second EE task is a positioning task of the EE as presented in the literature as state-of-the-art. Therefore, the coverage of the task surface

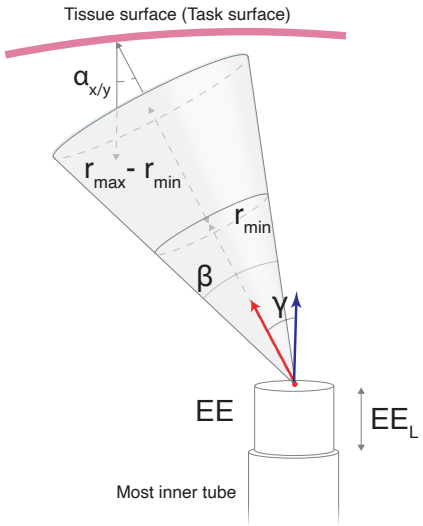

Fig. 3: The EE task in relation to the tissue surface (task surface) and the axial axis of the most inner tube (blue arrow). With $\alpha_{x/y}$ the angle between the task orientation vector and the tissue normal vector. β the angle of the field of operation and the operating angle γ described as the offset between the axial axis of the most inner tube (blue arrow) and the task orientation vector (red arrow).

is based on the Euclidean distance between the EE position and the task surface. The fifth EE configuration is configured again with r_{min} is 9 mm, r_{max} is 11 mm, EE_l is 10 mm, and the remaining EE parameters are not evaluated.

D. Optimization framework

1) Problem definition: The CTR design parameters (d) are the physical properties of the CTR; the radius of the curved section and the length of the curved section. The design space $\mathscr{D} \subset \mathbb{R}^n$, with n the number of scalar design parameters, holds an open set of all possible physical designs of the CTR. Furthermore, we assume that the CTR operates within the body cavity $\mathscr{W} := \mathbb{R}^3 \times \mathbb{S}^3$, with $\mathbb{S} = [0, 2\pi]$ and performs the EE task under the set constraints at task surface $\mathscr{S} \subset \mathscr{W}$.

The overall goal is to design a CTR which can perform the EE task under the set constraints at the complete task surface ($\mathscr{S}$) without interaction between the CTR and the tissue enclosing the workspace. Hereby, forming the optimization problem; finding the optimal design parameters $d^* \in \mathscr{D}$ which allow the EE task to be performed at the largest possible area of the task surface. The presented design problem is a continuous and volume-based and therefore solved in a discrete manner.

2) Discrete implementation: The discrete implementation is based on a RRT exploring the configuration space ($\mathscr{Q} := \mathbb{S}^m \times \mathbb{I}^m$) with m the number of tubes which can be rotated ($\mathbb{S}$) and translated ($\mathbb{I}$) during actuation; forming a single CTR configuration (q). The design parameters ($\mathscr{D}$) and the configuration space ($\mathscr{Q}$) can be mapped to the workspace and CTR body shapes for a given d by a kinematic model; $\mathscr{L}_d : \mathscr{Q} \rightarrow \mathscr{W}_d$, with $d \in \mathscr{D}$.

Two important subsets of configurations are contained within the configuration space ($\mathscr{Q}$), if the intersection between $\mathscr{W}_d$ and the body cavity formed by the urethra and the bladder is examined. First, a subset of configurations which do not cause tissue interaction under the current design parameters (d): $\mathscr{Q}_d^{free}$. As tissue interaction will apply external loading at unknown location(s) along the CTR body which results in unknown EE pose as the torsional free kinematic model ($\mathscr{L}_d$) cannot model external loading at unknown locations. The second subset is a set of configurations ($\mathscr{Q}_d^S$) which allow the EE task to be performed at the task surface ($\mathscr{S}$) under the set EE constraints. The intersection between these two configuration sets ($\mathscr{Q}_d^{EE} := \mathscr{Q}_d^S \cap \mathscr{Q}_d^{free}$) holds the configurations set ($\mathscr{Q}_d^{EE}$) without tissue interaction and which result in an EE pose at which the EE task covers a part of the task surface. The amount of coverage is denoted as the EE task coverage $C_d = [0,1]$ with $C_d = 1$ meaning that the EE task can be performed at the complete task surface ($\mathscr{S}$).

The design parameters d are updated with a Global Bounded Nelder-Mead (GBNM) algorithm [18] which is a derivative-free global bounded search method to minimize the object function. Therefore, the output of the EE task coverage function C_d is rewritten as a minimization function:

$$C_f = 1 - C_d. \tag{2}$$

The GBNM algorithm minimizes C_f by deploying local searchers, each with a probabilistic restart to search the design space $\mathscr{D}$. A spatial probability density is maintained of previous local searches to avoid local searchers finding the same local optima. Therefore, the resulting local optima provide the user with global optima, thus d^*.

3) Implementation: The RRT starts at the base of the path and grows towards the body cavity to ensure the CTR can reach the task surface without tissue interaction within the path. Configurations that result in CTR body shapes that cause tissue interaction are not included in $\mathscr{Q}$ which thereby directly forms $\mathscr{Q}_d^{free}$. This reduces the number of RRT iterations, because upcoming configurations drawn by the RRT are based on previously included configurations in state tree $\mathscr{Q}_d^{free}$ which ensures that the RRT only explores the body cavity itself.

As previously described the body cavity is computationally described by triangulating the path and the task surface in three edge faces. Each face in the task surface ($\mathscr{S}$) could be reduced to a point in space and a normal vector of this face, these surface points are denoted as $\mathscr{S}_p$. The number of surface points ($\mathscr{S}_p$) depends on the size of the task surface area and the area size of individual faces. As the RRT grows in the body cavity, the EE task under the set constraints is evaluated at the surface points. The EE task coverage (C_d) is denoted as the number of surface points ($\mathscr{S}_{pi}$) with i the number of points at which the EE task can be performed under the set constraints divided by the total number of surface points ($\mathscr{S}_{pt}$):

$$C_d = \frac{\mathscr{S}_{pi}}{\mathscr{S}_{pt}} \tag{3}$$

The final step is to update the design parameters d based on Equation 2 and 3 which form the object function of the GBNM algorithm and the local searchers. The GBNM local searchers run until either $C_d* = 1$ (the optimal design parameters are found), updating the design parameters d does not result in improvement ($< 0.1\%$ reduction of C_f) or a set number of updates is reached. The GBNM algorithm itself runs until either the optimal design parameters $d*$ are resulting in $C_d* = 1$ or a set number of local searchers have run.

The framework is implemented in C++ on an Apple MacBook Pro with an Apple M1 Max 10-core CPU. The first 5 % of the 200k RRT iterations are incremental then to decrease the computation time the RRT iterations are performed parallel in blocks of 50 configurations sets. A total of 25 local GBNM searchers are deployed during each optimization.

III. Results

As outlined in the previous section, the optimization framework has performed ten optimizations; five EE configurations in two body cavities. The average evaluation time to optimize the CTR design parameters for an EE configuration in a body cavity was 90.4 minutes. On average, 3976 sets of design parameters were evaluated distributed over the ten local searchers.

Table II presents the coverage of the task surface in body cavity A for sixteen cases. The design parameters were optimized for one EE configuration, but have also been applied to the other configuration to see the impact of EE configuration-dependent design optimization. The diagonal of the table (top left to bottom right) presents the optimal design parameters versus the EE configuration they were optimized for; this resulted in an average task surface coverage of 91.1 ± 3.5 %. The other cases present a set of optimized design parameters versus an EE configuration they were not optimized for, resulting in a lower average coverage of 77.1 ± 11.4 %.

TABLE II: The task surface coverage of the optimal design parameters ($d^*_{EE_{ci}}$) versus the four visualization EE configuration (EE_{ci}, $i = 1,2,3,4$) within body cavity A. Highlighted in bold are the optimal design parameter versus the EE configuration they are optimized for.

EE conf.	Parameter set			
	$d^*_{EE_{c1}}$	$d^*_{EE_{c2}}$	$d^*_{EE_{c3}}$	$d^*_{EE_{c4}}$
1	**93.8** %	91.8 %	58.5 %	78.6 %
2	90.6 %	**93.1** %	72.7 %	64.4 %
3	61.9 %	78.3 %	**86.0** %	74.2 %
4	91.3 %	85.2 %	78.1 %	**91.5** %

Similar to Table II, Table III presents the coverage of the task surface of body cavity B. The diagonal of the table shows an average coverage of the task surface of 19.4 ± 0.3 %. The other cases represent a set of optimal design parameters which is paired with an EE configuration which they are not optimized for showing an average coverage of 17.9 ± 1.3 %.

TABLE III: The task surface coverage of the optimal design parameters ($d^*_{EE_{ci}}$) versus the four visualization EE configuration (EE_{ci}, $i = 1,2,3,4$) within body cavity B. Highlighted in bold are the optimal design parameter versus the EE configuration they are optimized for.

EE conf.	Parameter set			
	$d^*_{EE_{c1}}$	$d^*_{EE_{c2}}$	$d^*_{EE_{c3}}$	$d^*_{EE_{c4}}$
1	**19.1** %	18.7 %	18.9 %	18.5 %
2	18.9 %	**19.4** %	19.1 %	19.0 %
3	16.2 %	18.4 %	**19.2** %	16.5 %
4	18.2 %	15.4 %	17.4 %	**19.7** %

Table IV presents the coverage of the task surface for ten cases, five cases for each body cavity. The design parameters are optimized for the fifth EE configuration which is based on the Euclidean distance between the EE position and the task surface. The optimal design parameter paired with the fifth EE configuration result in a 99.9 % coverage for body cavity A and 81.1 % for body cavity B. The optimal design paired with the other EE configurations result in a lower average coverage of 49.0 ± 2.4 % for body cavity A and 4.7 ± 1.0 % for body cavity B, a 50.5 % decrease in task surface coverage of body cavity A and 94.2 % for body cavity B.

TABLE IV: The task surface coverage of the optimal design parameters $d^*_{EE_{c5}}$ versus all five EE configuration (EE_{ci}, $i = 1,2,3,4,5$) within body cavity A and B (WS). Highlighted in bold is the coverage of the task surface if only the EE location is taken in account as show by the state-of-the-art.

WS	EE configuration				
	EE_{c1}	EE_{c2}	EE_{c3}	EE_{c4}	EE_{c5}
A	50.0 %	45.4 %	50.3 %	50.3 %	**99.9** %
B	3.4 %	5.3 %	4.6 %	5.6 %	**81.1** %

IV. Discussion

This study presents a framework that optimizes the design parameters of a CTR based on both the EE position and orientation in order to maximize the bladder wall area which can be visualized under the given EE constraints or in general

form that the coverage of the EE task is maximized over the task surface. Currently, the framework is optimized for bladder cancer using five EE configurations were defined: four EE configurations performed a visualization task of the bladder wall and a fifth performed a pure positioning task. These tasks were performed in two body cavities a simplified and realistic model of the urethra and bladder. This resulted in ten sets of optimal design parameters, one for each EE configuration versus a body cavity.

On average, the optimal design parameters for the visualization task lead to a $91.1 \pm 3.5\,\%$ coverage of the task surface in body cavity A and $19.4 \pm 0.3\,\%$ for body cavity B. In contrast, if a set of optimized parameters is deployed with another EE configuration, their coverage of the task surface dropped to an average of $77.1 \pm 11.4\,\%$ for body cavity A and $17.9 \pm 1.3\,\%$ for body cavity B. The decrease in task surface coverage for incorrect EE configurations is seen especially in body cavity A emphasizing the importance of adjusting the CTR design parameters for each EE task configuration.

The coverage of a complex task surfaces which comprises of small convex and concave radii is limited by Equation 1, these effects are seen if the coverage of body cavity B, a small radii body cavity (Table III) is compared with body cavity A, a large radii body cavity (Table II). Equation 1 sets a physical limit for the minimum radius the curved section of a tube can have and thereby limits the EE pose to obtain the correct orientation to perform the EE task along the complete task surface. Therefore, the coverage would benefit from a targeted or regional approach, this could allow for near perfect coverage of a region of interest, because the design parameters can be optimized to perform a task in that specific region. In clinical practice, this could result in near perfect coverage of a possible tumor location with advanced imaging techniques such as OCT.

Burgner et al. [11] and Baykal et al. [12] optimized the design parameters based on the Euclidean distance between the EE position and the task surface. However, as seen in Table IV this method is only valid if the EE task is based on the Euclidean distance between individual faces and the EE. Extending the functionality of the CTR with a dedicated EE task means that the optimization should also be extended to allow for this task as seen in the $72.4\,\%$ average decrease in coverage of fifth EE configuration versus the other four EE configurations. These results show that the CTR design parameters are task-dependent and should be optimized accordingly.

The accuracy of the current results may differ from the actual coverage during clinical practice, because the accuracy of the optimization is based on the task surface face size, the number of RRT iterations, local GBNM searchers, and the kinematic model. Increasing the face sizes and decreasing the RRT iterations and local searchers will decrease the accuracy but also computation time. Therefore, careful evaluation of these numbers is required to find a balance between the computation time (face sizes, RRT iterations and number of local searchers) and the accuracy of the design parameters.

Kinematic modeling of the CTR body is complex; bifurcation due to torsional windup and the effects of torsional and body stiffness influence the final EE pose. Therefore, the accuracy of the optimal design parameters partly depends on selecting the appropriate kinematic model. This work exploited the torsional free kinematic model due to its computational effectiveness, but more complex models, such as the torsional compliant model or models based on machine learning, can be integrated without changing the framework's structure. Implementing a more complex model could reduce the effects of bifurcation, torsional windup and body stiffness and thereby improve the accuracy of the framework.

The framework avoids configurations that cause tissue interaction, because it cannot be modeled by the torsional free kinematic model. However, during clinical practice tissue interaction does not cause problems as the compliant CTR body will not cause tissue damage. As a result configuration sets which are excluded due to tissue interaction during simulation could result in task surface coverage during clinical practice, which theoretically can increase the overall coverage of a given set of design parameters.

Therefore, we recommend that future studies will focus on two parts of the simulation; improvement of the kinematic modeling by using the torsional compliant model and robot specific models, and the clinical side of the simulation. The current computation time of 90.4 minutes is already promising to embed in the pre-operative clinical workflow. However, representative phantom based experiments are needed to validate the difference between simulated coverage and coverage during clinical practice.

V. Conclusion

This paper presents a computational design framework that optimizes the CTR design parameters for a specific workspace, EE task, and EE configuration. The workspace is a body cavity, in our case, the lower urinary tract (urethra and bladder). The EE task is described by eight EE constraints for an EE configuration, this allows for a general task description making the framework applicable to a large range of EE tasks. The optimization framework uses these constraints to optimize a three tube CTR with six design parameters; the radius and the length of the curved section of the three individual tubes. The optimal CTR design parameters maximize the coverage of the EE task on the task surface.

The framework is demonstrated by optimizing the design parameters of a CTR for five EE configurations; four configurations visualize the bladder wall, and the fifth configuration performs a positioning task as presented in literature. The fifth EE configuration shows that extending the EE task from a pure positioning task to a clinical relevant task such as a visualization of the bladder wall greatly reduce the coverage of the task surface. The four EE configurations which visualize the bladder wall show that a set of design parameters that works well for one EE configuration, perform less for other configurations. Therefore, our work underlines the importance of adaptation to the body cavity, but also shows the importance of taking the task constraints and EE configuration into account when designing a CTR.

REFERENCES

[1] A. Richters, K. K. Aben, and L. A. Kiemeney, "The global burden of urinary bladder cancer: an update," *World Journal of Urology*, vol. 38, no. 8, pp. 1895–1904, 2020.

[2] M. C. Kriegmair, T. Bergen, M. Ritter, P. Mandel, M. S. Michel, T. Wittenberg, and C. Bolenz, "Digital Mapping of the Urinary Bladder: Potential for Standardized Cystoscopy Reports," *Urology*, vol. 104, pp. 235–241, 2017. [Online]. Available: http://dx.doi.org/10.1016/j.urology.2017.02.019

[3] N. Falcon, S. Ranjbar, E. Cisneros, B. Vu, A. Schoppe, P. Sanchez, Y.-F. Jin, J. Y. Ye, Y. Feng, D. Kaushik, and R. L. Hood, "Innovative computer vision approach to 3D bladder model reconstruction from flexible cystoscopy," *Proc. SPIE 10852, Therapeutics and Diagnostics in Urology*, vol. 1085207, no. February 2019, p. 6, 2019.

[4] D. P. Popescu, L. P. Choo-Smith, C. Flueraru, Y. Mao, S. Chang, J. Disano, S. Sherif, and M. G. Sowa, "Optical coherence tomography: Fundamental principles, instrumental designs and biomedical applications," *Biophysical Reviews*, vol. 3, no. 3, pp. 155–169, 2011.

[5] G. Fananapazir, A. Kitich, R. Lamba, S. L. Stewart, and M. T. Corwin, "Normal reference values for bladder wall thickness on CT in a healthy population," *Abdominal Radiology*, vol. 43, no. 9, pp. 2442–2445, 2018. [Online]. Available: https://doi.org/10.1007/s00261-018-1463-x

[6] Z. Li, L. Wu, H. Ren, and H. Yu, "Kinematic comparison of surgical tendon-driven manipulators and concentric tube manipulators," *Mechanism and Machine Theory*, vol. 107, no. September 2016, pp. 148–165, 2017. [Online]. Available: http://dx.doi.org/10.1016/j.mechmachtheory.2016.09.018

[7] C. Bedell, J. Lock, A. Gosline, and P. E. Dupont, "Design optimization of concentric tube robots based on task and anatomical constraints," in *2011 IEEE International Conference on Robotics and Automation*, vol. 31, no. 1. IEEE, may 2011, pp. 398–403. [Online]. Available: http://ieeexplore.ieee.org/document/5979960/

[8] J. Burgner-Kahrs, H. B. Gilbert, J. Granna, P. J. Swaney, and R. J. Webster, "Workspace characterization for concentric tube continuum robots," *IEEE International Conference on Intelligent Robots and Systems*, no. Iros, pp. 1269–1275, 2014.

[9] C. Bergeles, A. H. Gosline, N. V. Vasilyev, P. J. Codd, P. J. Del Nido, and P. E. Dupont, "Concentric tube robot design and optimization based on task and anatomical constraints," *IEEE Transactions on Robotics*, vol. 31, no. 1, pp. 67–84, 2015.

[10] J. T. Lin, C. Girerd, J. Yan, J. T. Hwang, and T. K. Morimoto, "A generalized framework for concentric tube robot design using gradient-based optimization," *IEEE Transactions on Robotics*, vol. 38, pp. 3774–3791, 12 2022.

[11] J. Burgner, H. B. Gilbert, and R. J. Webster, "On the computational design of concentric tube robots: Incorporating volume-based objectives," *Proceedings - IEEE International Conference on Robotics and Automation*, pp. 1193–1198, 2013.

[12] C. Baykal, C. Bowen, and R. Alterovitz, "Asymptotically optimal kinematic design of robots using motion planning," *Autonomous Robots*, vol. 43, no. 2, pp. 345–357, feb 2019. [Online]. Available: http://link.springer.com/10.1007/s10514-018-9766-x

[13] L. G. D. Veras, F. L. Medeiros, and L. N. Guimaraes, "Systematic Literature Review of Sampling Process in Rapidly-Exploring Random Trees," *IEEE Access*, vol. 7, pp. 50 933–50 953, 2019.

[14] L. Ingber, "Adaptive simulated annealing (ASA)," *Global optimization C-code, Caltech Alumni Association, Pasadena, CA*, 1993.

[15] R. De Robertis, B. Maris, N. Cardobi, P. T. Martini, S. Gobbo, P. Capelli, S. Ortolani, S. Cingarlini, S. Paiella, L. Landoni, G. Butturini, P. Regi, A. Scarpa, G. Tortora, and M. D'onofrio, "Can histogram analysis of mr images predict aggressiveness in pancreatic neuroendocrine tumors?" *European Radiology*, vol. 28, no. 6, pp. 2582–2591, 2018.

[16] R. J. Webster, J. M. Romano, and N. J. Cowan, "Mechanics of precurved-tube continuum robots," *IEEE Transactions on Robotics*, vol. 25, no. 1, pp. 67–78, 2009.

[17] T. K. Morimoto and A. M. Okamura, "Design of 3-D printed concentric tube robots," *IEEE Transactions on Robotics*, vol. 32, no. 6, pp. 1419–1430, 2016.

[18] M. A. Luersen and R. Le Riche, "Globalized nelder-mead method for engineering optimization," *Computers and Structures*, vol. 82, no. 23-26, pp. 2251–2260, 2004.